

## CO Dissociation on Model Co/SiO<sub>2</sub> Catalysts – Effect of Adsorbed Hydrogen

Michael E. Floto<sup>†</sup>, Ryan A. Ciufu<sup>†</sup>, Sungmin Han<sup>†</sup>, and C. Buddie Mullins<sup>\*‡</sup>

<sup>†</sup> Department of Chemistry, The University of Texas at Austin, Austin, Texas 78712, United States

<sup>‡</sup> McKetta Department of Chemical Engineering, Texas Materials Institute, Center for Electrochemistry, The University of Texas at Austin, Austin, Texas 78712, United States

### ABSTRACT

We found experimental evidence that shows the effect that adsorbed hydrogen can have on CO dissociation. For cobalt nanoparticles supported on SiO<sub>2</sub>, adsorbed hydrogen enhances CO dissociation. In contrast, adsorbed hydrogen inhibits CO dissociation on a cobalt film supported on SiO<sub>2</sub>. Considering the nature of cobalt deposited by physical vapor deposition, these results can be explained by a preference for CO dissociation to follow the hydrogen-assisted dissociation mechanism on FCC cobalt and step-edges, while the direct dissociation mechanism is preferred on HCP cobalt. These results are in agreement with previous theoretical results.

KEYWORDS: CO dissociation, mechanism, Fischer-Tropsch synthesis, hydrogen, temperature programmed desorption

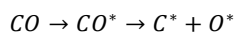
### 1. Introduction

Carbon monoxide (CO) dissociation is a crucial step in the Fischer-Tropsch Synthesis (FTS) process.<sup>1</sup> FTS produces hydrocarbons from a mixture of CO and hydrogen gas (H<sub>2</sub>), known as synthesis gas, to be used as chemical feed-stocks or fuels.<sup>2</sup> Synthesis gas comes from coal, natural gas, or biomass, allowing for a sustainable source of energy relevant products and the opportunity to mitigate the need for petroleum based sources.<sup>3</sup> FTS has been studied extensively in industry and academia, however there still lacks a well-established fundamental understanding of the reaction mechanism.<sup>4</sup> Revealing fundamental information about FTS will help push this process forward in becoming more efficient and useful. The current study aims to provide a clearer understanding of CO dissociation on cobalt, a widely used metal catalyst for industrial FTS processes.<sup>2</sup> The experimental research reported here was performed by studying CO dissociation under ultra-high vacuum (UHV) conditions on model surfaces of cobalt supported on silica (SiO<sub>2</sub>), a commonly used support for cobalt catalysts.<sup>2</sup>

The proposed mechanisms under consideration for CO dissociation during FTS are direct and hydrogen-assisted (H-assisted) dissociation.<sup>1,5-12</sup> The direct dissociation mechanism involves metal interaction with chemisorbed CO (CO\*), resulting in dissociation into chemisorbed carbon (C\*) and oxygen (O\*). The H-assisted dissociation mechanism involves CO\* interaction with the metal surface as well as chemisorbed hydrogen (H\*)<sup>13,14</sup> to form an intermediate (HCO\* and/or COH\*), resulting in dissociation into C\*/CH\* and O\*/OH\*. These mechanism details are summarized in Scheme 1 below.

**Scheme 1.** Elementary steps for direct and H-assisted CO dissociation.

**Direct dissociation:**



**H-assisted dissociation:**



There are several theoretical studies of CO dissociation on cobalt.<sup>5-8,11,12</sup> One in particular by Liu *et al.* studied the crystallographic dependence of CO dissociation on cobalt catalysts.<sup>5</sup> This study showed CO dissociation on hexagonal-closed-packed (HCP) cobalt catalysts to be more facile through the direct dissociation route, while dissociation on face-centered-cubic (FCC) cobalt catalysts is more facile through the hydrogen-assisted route. Additionally, a computational study by Ciobîcă *et al.* showed the hydrogen-assisted dissociation route to be thermodynamically preferred for CO dissociation on step-edge sites (or coordinatively unsaturated surface cobalt atoms) of cobalt catalysts.<sup>12</sup>

Cobalt metal will primarily exist in the HCP or the FCC crystal structure. Under standard conditions, bulk cobalt will thermodynamically prefer to exist with an HCP structure until heated above 700 K at which point FCC cobalt is more stable.<sup>15</sup> Cobalt, along with other transition metals, deposited at low coverages onto a metal oxide support using

physical vapour deposition (PVD) techniques such as in the current study have been shown to reliably form as small particles at room temperature and/or with an annealing step.<sup>16-19</sup> Cobalt nanoparticles formed by PVD under vacuum behave differently from bulk cobalt with regard to crystal structure. Cobalt nanoparticles (< 100 nm) formed from PVD result in predominately FCC cobalt.<sup>20-32</sup> The preference for cobalt nanoparticles made from physical routes to exist as FCC cobalt is argued to be a result of thermal history involved during particle formation and lattice strain effects on small nanoparticles.<sup>33</sup> As cobalt nanoparticles get larger (> 100 nm) or form continuous films, they behave like bulk cobalt with regard to their crystal structure and exist predominately as HCP cobalt.<sup>34-36</sup> Another important structural difference from cobalt nanoparticles and bulk cobalt films is the abundance of surface defects such as step-edges. Metal nanoparticles are known to have higher surface defect concentrations than bulk metal.<sup>37</sup> These structural considerations of cobalt catalysts play a crucial role for their activity towards CO dissociation.

Herein, CO dissociation was studied on model catalysts comprised of cobalt nanoparticles or a cobalt film supported on silica. This approach allows for the study of an industrially relevant model surface as opposed to the single crystalline cobalt samples used in many model studies, which suffer a significant materials gap to “real world” catalysts.<sup>38</sup> Cobalt-based catalysts in industrial applications for FTS often exist as cobalt nanoparticles supported on silica.<sup>39</sup> The current surface science study under UHV conditions allows us to understand molecular level catalytic interactions of various molecules by adopting surface and gaseous analysis techniques such as temperature programmed desorption (TPD) and Auger electron spectroscopy (AES), not possible under the harsh conditions of high pressure reactor cells. There is little experimental evidence for the CO dissociation mechanism on cobalt that is conclusive and in some cases, the findings are contradictory.<sup>10,11</sup> To the best of our knowledge, the current study provides the first conclusive experimental evidence for the CO dissociation mechanism on cobalt model surfaces supported on silica.

## 2. Materials and methods

All experiments in this study were performed in a UHV chamber with a base pressure of  $1 \times 10^{-10}$  Torr, described in detail in the Supplementary Information (SI) and previous studies.<sup>40,41</sup> In short, this chamber is equipped with a quadrupole mass spectrometer (QMS) for detecting gaseous species, and AES for surface elemental identification. The sample supporting substrate, a 9 by 9 mm tantalum (Ta) foil that is 0.5 mm thick, is mounted by spot welding to a probe attached to a manipulator with x, y, z, and rotational freedom. The probe can be filled with liquid nitrogen to cool the sample to 77 K and it can also be resistively heated by a direct current power supply up to 1000 K. The temperature of the sample was measured by a K-type (alumel-chromel) thermocouple spot welded to the back of the Ta substrate. Argon ion bombardment (1 keV), followed by annealing to 1000 K was performed to clean the Ta sample as confirmed by AES.

The model Co/SiO<sub>2</sub> catalysts were prepared by first depositing a film of SiO<sub>2</sub> onto a clean Ta sample. The technique used for depositing SiO<sub>2</sub> was replicated from that of Goodman *et al.*<sup>42</sup> Briefly, a silicon rod (1 mm dia., 1 cm length) was wrapped by Ta wire (0.5 mm dia.). The Ta wire was resistively heated until the Si rod was hot enough to evaporate. The silicon was evaporated in  $1 \times 10^{-5}$  Torr of O<sub>2</sub> followed by annealing of the substrate to 850 K, resulting in deposition of SiO<sub>2</sub>, as confirmed by AES. With a thin film of SiO<sub>2</sub> covering the Ta substrate, cobalt was then deposited by electron-beam evaporation, with the mono layer (ML) coverage calibrated by a quartz crystal microbalance (QCM) and assuming the thickness of 1 ML to be the diameter of a Co atom (0.25 nm). For cobalt nanoparticles (2 ML), the sample was annealed to 700 K for 10 minutes to ensure the formation of cobalt nanoparticles.<sup>43</sup> For cobalt films (20 ML) the sample was annealed to 500 K to desorb background gas molecules. TPD measurements were performed after exposing the Co/SiO<sub>2</sub> surfaces to solely CO or to H<sub>2</sub> followed by CO at 300 K followed by heating the sample up to 900 K (5 K/s). Each sample was cleaned and redeposited after every TPD measurement.

## 3. Results & Discussion

AES measurements of the model surfaces employed in this study are shown in Figure 1. The black curve shows an AES spectra of the Ta substrate with Auger features at 168 and 178 eV. A 30 minute SiO<sub>2</sub> deposition results in the AES curve in red, showing a strong signal for SiO<sub>2</sub> at 80 eV, as well as mostly undetectable Ta features. Based on the profile depth of AES, this result confirms the SiO<sub>2</sub> film to be at least 5 nm thick,<sup>44</sup> more than thick enough to eliminate charge transfer between cobalt and the underlying Ta substrate.<sup>45</sup> SiO<sub>2</sub> deposition of 30 minutes was chosen for silica films upon which cobalt was deposited. The blue curve shows the AES spectra of 2 ML of cobalt deposited and annealed (700 K, 10 min) on a silica film, with Auger features for cobalt at 660, 721, and 781 eV. The growth mechanism of cobalt deposition on silica at room temperature has been shown to be layer-by-layer growth at room temperature while forming islands after annealing.<sup>43</sup> Auger measurements of increasing deposition of cobalt on a SiO<sub>2</sub>/Ta substrate with and without annealing showed similar results (Figure 3S.). The size and distribution of the cobalt nanoparticles resulting from this process was characterized previously by Goodman *et al.*<sup>46</sup> using transmission electron microscopy (TEM). A 2 ML annealed cobalt deposition on SiO<sub>2</sub> resulted in cobalt nanoparticles about 5 nm in diameter. For the cobalt film (green curve), 20 ML of cobalt was deposited on a silica film. Intense Co Auger features are observed, while

the SiO<sub>2</sub> feature is undetectable resulting from the continuous cobalt film (~ 5 nm thick). The goal in this study is to compare the effect of adsorbed hydrogen on the activity for CO dissociation between cobalt films (> 1.25 nm thick) and cobalt nanoparticles (< 20 nm in diameter) supported on silica. Based on the work done by Goodman *et al.* and the similar experimental setup in the current study, as well as the AES measurements in this study we believe that a 2 ML cobalt deposition with annealing and 20 ML cobalt deposition results in cobalt nanoparticles (< 20 nm) and a cobalt film (> 1.25 nm) on a silica surface, respectively.

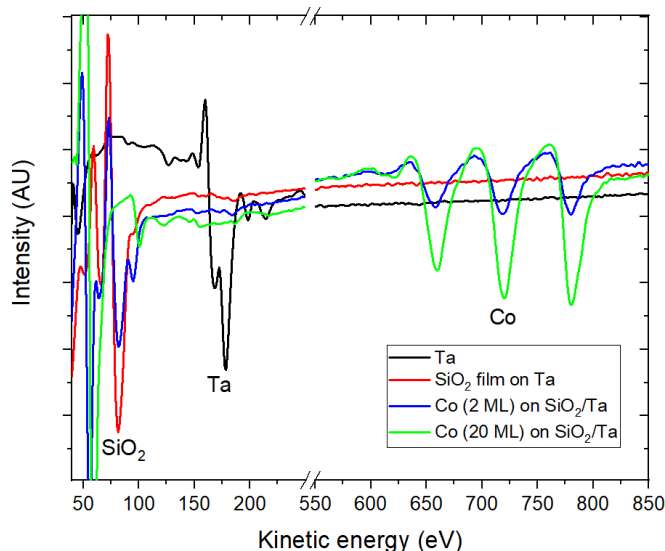


**Figure 1.** AES spectra of Ta substrate (black), SiO<sub>2</sub> film (red), Co (2 ML) on SiO<sub>2</sub>/Ta, and Co (20 ML) on SiO<sub>2</sub>/Ta (green)

Auger measurements were made on a silica film, cobalt nanoparticles on silica after preparation, and cobalt nanoparticles on silica after intentional oxidation ( $1 \times 10^{-5}$  Torr O<sub>2</sub>, 700 K, 5 min.) in order to address the nature of cobalt nanoparticles prepared on silica. The resulting Auger spectra showing the oxygen Auger lines are shown in Figure 2. We focus on the oxygen signal, because this signal results from the KVV Auger electron transitions of oxygen which involve valence electrons and can thus provide chemical state information of oxygen based on the kinetic energy value (eV) of that feature.<sup>47</sup> Namely there is a shift to higher energy going from silica to cobalt oxide by about 4.6 eV. In Figure 2, the black curve shows the oxygen feature from the silica film around 507 eV. The red curve shows the oxygen feature for as-prepared cobalt nanoparticles on silica around 507.7 eV. The shift to higher energy by 0.7 eV is likely due to cobalt interaction with oxygen at the interface of the silica film and the cobalt nanoparticles. The signal intensity decrease is likely a result of metallic cobalt blocking detection of some of the KVV transition Auger electrons from oxygen in the underlying silica layer. The blue curve shows the oxygen feature of the cobalt nanoparticles on silica after intentional oxidation ( $1 \times 10^{-5}$  Torr O<sub>2</sub>, 700 K, 5 min.). The signal shifts to 510 eV and increases in intensity. The shift to higher energy and increased intensity is due to increased cobalt interaction with oxygen as a result of oxidation of the metallic cobalt. These results provide evidence for the nature of as-prepared cobalt nanoparticles to be metallic. These results are in agreement with similar measurements made by Goodman *et al.* on cobalt nanoparticles supported on silica.<sup>46</sup>

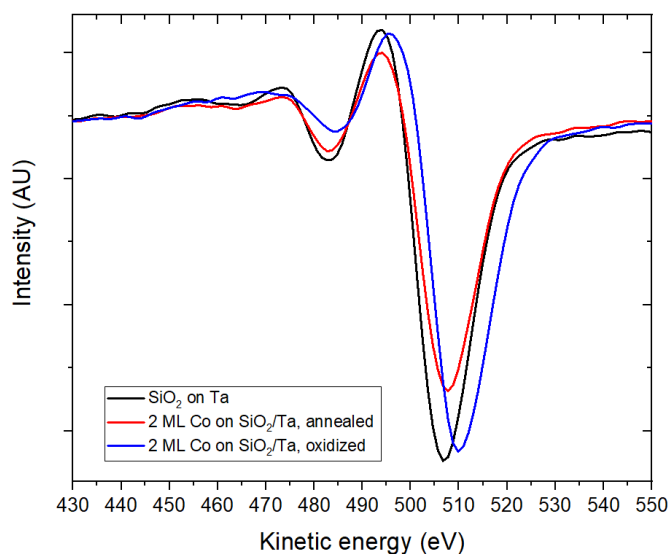


**Figure 2.** Oxygen Auger lines for a silica film (black), as-prepared cobalt nanoparticles on silica (red), and oxidized cobalt nanoparticles on silica (blue).

TPD measurements were conducted in order to study CO dissociation on cobalt and the effect of adsorbed hydrogen, the results of which are shown in Figure 3 (further explanation of this measurement in the SI). The black curve shows the TPD results for the cobalt film exposed to 1 L CO. The desorption feature just below 450 K comes from molecular CO desorption, while the feature above 550 K comes from the associative desorption of CO from C\* and O\* as a result of CO dissociation.<sup>48,49</sup> When the Co film is exposed to 1 L H<sub>2</sub>, followed by 1 L CO (red curve), the same peaks are observed, with a significant decrease from the black curve in associative CO desorption. It is worth noting the CO desorption curve for the cobalt films resembles that of polycrystalline HCP cobalt.<sup>53</sup> The blue curve shows the TPD curve for cobalt nanoparticles exposed to 1 L CO. There appears to be mostly molecular CO desorbing with a peak around 380 K and very little associative desorption above 800 K. For cobalt nanoparticles exposed to 1 L H<sub>2</sub>, followed by 1 L CO (green curve), molecular CO desorbs around 380 K and there is a significant increase compared with the blue curve regarding associative CO desorption at 800 K. The small peaks for associative desorption for the cobalt nanoparticles can be explained by alternative paths for the CO-derived carbon. Namely, carbon can diffuse into the SiO<sub>2</sub> support upon heating and bind irreversibly to the underlying Ta,<sup>50</sup> and carbon can bind strongly to defect sites of cobalt and deactivate those sites by not being removed.<sup>51</sup>

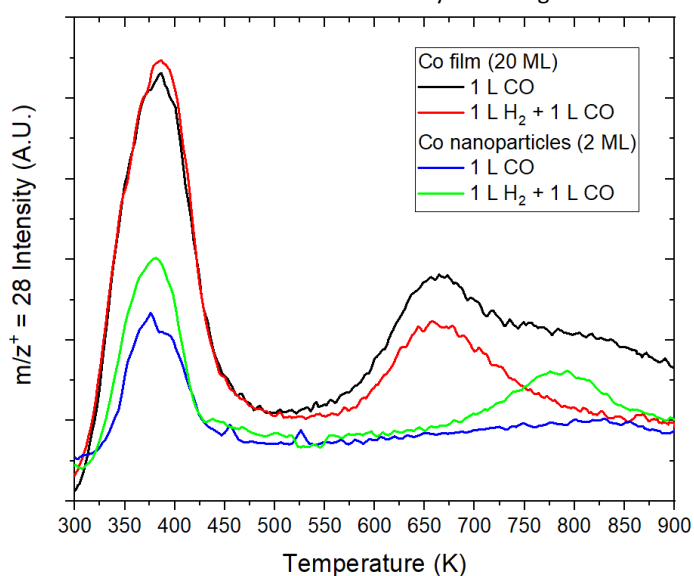


### Figure 3. TPD curves for Co film and Co nanoparticles

The associative desorption feature for cobalt nanoparticles (800 K) is at a higher temperature than that of cobalt films (660 K). We argue this to be caused by a combination of stronger interaction of C\* and O\* with cobalt nanoparticles compared to bulk cobalt. Namely, C\* and O\* will bind strongly to the abundant step-edges of cobalt.<sup>51,52</sup> Stronger interactions of C\* and O\* with cobalt nanoparticles will require more energy required for associative desorption, as seen in the TPD data.

For the cobalt films and nanoparticles, it appears H\* has a significant effect on associative desorption of CO. There is a decrease in associative desorption on the cobalt films upon exposure to H<sub>2</sub> + CO compared to that with only CO exposure. This result indicates that CO dissociation is inhibited by the presence of H\* on the cobalt films, possibly due to the preferred mechanism for CO dissociation. With H\* present on the surface, some CO molecules are likely to form some intermediate with H\* (HCO\* and/or COH\*), requiring dissociation to go about the H-assisted mechanism. If CO on cobalt films prefers direct over H-assisted dissociation, then interaction with H\* would result in less CO dissociation, which is observed in the TPD data. On the contrary, for the cobalt nanoparticles, there is an increase in associative desorption with H<sub>2</sub> + CO exposure compared to that with only CO exposure. These affects were shown to be reproducible (Figure 1S). This result shows that CO dissociation is enhanced by the presence of H\*, possibly due to the preferred CO dissociation mechanism. If CO on cobalt nanoparticles prefers H-assisted over direct CO dissociation, then interaction with H\* would result in more CO dissociation, which is observed in the TPD data. The difference in CO dissociation mechanism preference between the cobalt film and particles is likely due to structural differences such as crystallinity and defect concentration. Previous computational studies have shown thermodynamic preference for the mechanism of CO dissociation on cobalt catalysts based on these structural details. The theoretical study by Liu *et al.* mentioned previously showed direct CO dissociation to be favoured on HCP cobalt catalysts and H-assisted dissociation to be favoured on FCC cobalt catalysts.<sup>5</sup> Additionally, calculations showed step-edge sites on cobalt to favour H-assisted CO dissociation over that of direct dissociation.<sup>12</sup> Considering cobalt nanoparticles (< 100 nm) prepared by PVD techniques consist of mostly FCC cobalt,<sup>20-32</sup> while that of cobalt films/bulk consist mostly of HCP cobalt,<sup>34-36</sup> and cobalt nanoparticles have a higher concentration of surface defects compared to that of bulk cobalt films,<sup>37</sup> the results of the current study provide experimental evidence in agreement with theoretical results from literature.

#### 4. Conclusion

In conclusion, the results of this study shed light on the dissociation of CO, a crucial step in FTS, on cobalt catalysts. By controlling the quantity of cobalt deposited on silica, we observed different catalytic activities for CO dissociation on cobalt films and cobalt nanoparticles. The results show CO dissociation to be inhibited by the presence of H\* on cobalt films, suggesting the preferred mechanism to be direct CO dissociation on cobalt films (~ 5 nm thick). For cobalt nanoparticles however, the presence of H\* enhanced CO dissociation, suggesting the preferred mechanism to be H-assisted CO dissociation on cobalt nanoparticles (~ 5 nm dia.). Considering the surface structure of cobalt nanoparticles (<100 nm) and cobalt films (> 1.25 nm), these results can be explained by previous calculations that show H-assisted CO dissociation to be preferred on FCC cobalt and cobalt step-edge sites, while direct CO dissociation to be preferred on HCP cobalt.<sup>5,12</sup> This study provides a clearer understanding of CO dissociation on cobalt surfaces and can be used to improve FTS when considering the effect of hydrogen and the structure of cobalt.

#### Conflicts of interest

There are no conflicts of interest to declare.

#### Acknowledgements

We are thankful for the generous support of the Department of Energy, Basic Energy Sciences, Catalysis Science Program (Grant DE- SC0018116) and the Welch Foundation (Grant F1436).

#### Notes and references

- 1 S. Shetty and R. A. Van Santen, *Catal. Today*, 2011, **171**, 168-173.
- 2 H. Mahmoudi, M. Mahmoudi, O. Doustdar, H. Jahangiri, A. Tsolakis, S. Gu and M. LechWyszynski, *Biofuels Eng.*, 2018, **2**, 11-31.
- 3 H. Jahangiri, J. Bennett, P. Mahjoubi, K. Wilson and S. Gu, *Catal. Sci. Technol.*, 2014, **4**, 2210-2229.

- 4 R. A. Van Santen, A. J. Markvoort, I. A. W. Filot, M. M. Ghouri and E. J. M. Hensen, *Phys. Chem. Chem. Phys.*, 2013, **15**, 17038-17063.
- 5 J. X. Liu, H. Y. Su, D. P. Sun, B. Y. Zhang and W. X. Li, *J. Am. Chem. Soc.*, 2013, **135**, 16284-16287.
- 6 M. Ojeda, R. Nabar, A. U. Nilekar, A. Ishikawa, M. Mavrikakis and E. Iglesia, *J. Catal.*, 2010, **272**, 287-297.
- 7 M. A. Petersen, J. A. Van Den Berg, I. M. Ciobîcă and P. Van Helden, *ACS Catal.*, 2017, **7**, 1984-1992.
- 8 O. R. Inderwildi, S. J. Jenkins and D. A. King, *J. Phys. Chem. C.*, 2008, **112**, 1305-1307.
- 9 M. Ojeda, A. Li, R. Nabar, A. U. Nilekar, M. Mavrikakis and E. Iglesia, *J. Phys. Chem. C.*, 2010, **114**, 19761-19770.
- 10 W. Chen, B. Zijlstra, I. A. W. Filot, R. Pestman and E. J. M. Hensen, *Chem. Cat. Chem.*, 2018, **10**, 136-140.
- 11 A. Tuxen, S. Carenco, M. Chintapalli, C. Chuang, C. Escudero, E. Pach, P. Jiang, F. Borondics, B. Beberwyck, A. P. Alivisatos, G. Thornton, W. Pong, J. Guo, R. Perez, F. Besenbacher and M. Salmeron, *J. Am. Chem. Soc.*, 2013, **135**, 2273-2278.
- 12 P. Van Helden, J. A. Van Den Berg and I. M. Ciobîcă, *Catal. Sci. Technol.*, 2012, **2**, 491-494.
- 13 R. Duš and W. Lisowski, *Surf. Sci.*, 1976, **61**, 635-645.
- 14 R. M. Bridge, M. E., Comrie, C. M., Lambert, *J. Catal.*, 1979, **58**, 28-33.
- 15 M. Hansen, R. P. Elliot, and F. A. Shunk, *Constitution of binary alloys*, New York, 1958.
- 16 M. Baumer and H. Freund, *Prog. Surf. Sci.*, 1999, **61**, 127-198.
- 17 D. R. Rainer and D. W. Goodman, *J. Mol. Catal. A Chem.*, 1998, **131**, 259-283.
- 18 D. R. Rainer, C. Xu and D. W. Goodman, *J. Mol. Catal. A Chem.*, 1997, **119**, 307-325.
- 19 C. C. Chusuei, X. Lai, K. Luo and D. W. Goodman, *Top. Catal.*, 2000, **14**, 71-83.
- 20 C. G. Granqvist and R. A. Buhrman, *J. Appl. Phys.*, 1976, **47**, 2200-2219.
- 21 W. Gong, H. Li, Z. Zhao and J. Chen, *J. Appl. Phys.*, 1991, **69**, 5119-5121.
- 22 E. Anno, *Phys. Rev. B*, 1994, **50**, 17502-17506.
- 23 Y. S. O. Kitakami, T. Sakurai, Y. Miyashita, Y. Takeno, Y. Shimada, H. Takano, H. Awano, K. Ando, *Jpn. J. Appl. Phys.*, 1996, **35**, 1724-1728.
- 24 V. Skumryev, S. Stoyanov, Y. Zhang, G. Hadjipanayis, D. Givord and J. Nogués, *Nature*, 2003, **423**, 850-853.
- 25 R. Katoh, T. Hihara, D. L. Peng and K. Sumiyama, *Appl. Phys. Lett.*, 2003, **82**, 2688-2690.
- 26 X. L. Dong, Z. D. Zhang, Y. C. Chuang and S. R. Jin, *Phys. Rev. B - Condens. Matter Mater. Phys.*, 1999, **60**, 3017-3020.
- 27 J. Jiao, S. Seraphin, X. Wang and J. C. Withers, *J. Appl. Phys.*, 1996, **80**, 103-108.
- 28 S. Kajiwara, S. Ohno and K. Honma, *Philos. Mag. A*, 1991, **63**, 625-644.
- 29 X. G. Li, T. Murai, A. Chiba and S. Takahashi, *J. Appl. Phys.*, 1999, **86**, 1867-1873.
- 30 O. Kitakami, H. Sato, Y. Shimada, F. Sato and M. Tanaka, *Phys. Rev. B*, 1997, **56**, 849-854.
- 31 P. Van Helden, I. M. Ciobîcă and R. L. J. Coetzer, *Catal. Today*, 2016, **261**, 48-59.
- 32 K. Kimoto, Y. Kamiya, M. Nonoyama and R. Uyeda, *Jpn. J. Appl. Phys.*, 1963, **2**, 702-713.
- 33 X. Q. Zhao, S. Veintemillas-Verdaguer, O. Bomati-Miguel, M. P. Morales and H. B. Xu, *Phys. Rev. B*, 2005, **71**, 1-7.
- 34 C. Rath and J. Prieto, S. Muller, R. Miranda, and K. Heinz, *Phys. Rev. B*, 1997, **55**, 10791-10799.
- 35 D. Renard and G. Nihoul, *Philos. Mag. B*, 1987, **55**, 75-86.
- 36 K. Le Dang, P. Veillet, C. Chappert, P. Beauvillain and D. Renard, *J. Phys. F: Met. Phys.* 1986, **16**, L109 - L112.
- 37 M. Salis, C. M. Carbonaro, M. Marceddu and P. C. Ricci, *Nanosci. Nanotechnol.*, 2013, **3**, 27-33.
- 38 T. P. St.Clair and D. W. Goodman, *Top. Catal.*, 2000, **13**, 5-19.
- 39 A. Y. Khodakov, *Catal. Today*, 2009, **144**, 251-257.
- 40 B. A. Ferguson, C. T. Reeves, and C. B. Mullins, *J. Chem. Phys.*, 1999, **110**, 11574-11584.
- 41 M. C. Wheeler, D. C. Seets and C. B. Mullins, *J. Chem. Phys.*, 1996, **105**, 1572-1583.
- 42 Z. Yan, Z. Wang, D. B. Bukur and D. W. Goodman, *J. Catal.*, 2009, **268**, 196-200.
- 43 J. Čechal, J. Luksch, K. Koňáková, M. Urbánek, E. Brandejsová and T. Šikola, *Surf. Sci.*, 2008, **602**, 2693-2698.
- 44 G. U. Pignatelli and G. Queirolo, *Radiat. Eff.*, 1983, **79**, 291-303.
- 45 A. Sandell, J. Libuda, P. Brühwiler, S. Andersson, A. Maxwell and N. Martensson, *Phys. Rev. B.*, 1997, **55**, 7233-7243.
- 46 Z. Wang, S. Skiles, F. Yang, Z. Yan and D. W. Goodman, *Catal. Today*, 2012, **181**, 75-81.
- 47 C. D. Wagner, D. A. Zatko and R. H. Raymond, *Anal. Chem.*, 1980, **52**, 1445-1451.
- 48 U. Bardi, P. Tiscione and G. Rovida, *Appl. Surf. Sci.*, 1986, **27**, 299-317.
- 49 K. A. Prior, E. G. Scott and R. M. Lambert, *Chem. Phys. Lett.*, 1981, **80**, 517-520.
- 50 I. Mizushima, E. Kamiya, N. Arai, M. Sonoda, M. Yoshiki, S. Takagi, M. Wakamiya, S. Kambayashi, Y. Mikata, S. Mori and M. Kashiwagi, *Jpn. J. Appl. Phys.*, 1997, **36**, 1465-1468.
- 51 J. Nakamura, I. Toyoshima, and K. Tanaka, *Surf. Sci.*, 1988, **201**, 185-194.
- 52 C. J. Weststrate, P. Van Helden, J. Van De Loosdrecht and J. W. Niemantsverdriet, *Surf. Sci.*, 2016, **648**, 60-66.
- 53 M. E. Bridge and R. M. Lambert, *Surf. Sci.*, 1979, **82**, 413-424.
- 54 G. Attard and C. Barnes, *Surfaces*, New York, 1998

## H\*-assisted



Co nanoparticles



## Direct



Co film

